

Air plasma waveguide using pico-sec and nano-sec laser pulses

Pramod K. Pandey, Shyam L. Gupta, V. Narayanan, and Raj K. Thareja

Citation: *Physics of Plasmas* (1994-present) **19**, 023502 (2012); doi: 10.1063/1.3676617

View online: <http://dx.doi.org/10.1063/1.3676617>

View Table of Contents: <http://scitation.aip.org/content/aip/journal/pop/19/2?ver=pdfcov>

Published by the [AIP Publishing](#)

Articles you may be interested in

[Plasma expansion into a waveguide created by a linearly polarized femtosecond laser pulse](#)

Phys. Plasmas **20**, 063102 (2013); 10.1063/1.4810797

[Long-distance directed transfer of microwaves in tubular sliding-mode plasma waveguides produced by KrF laser in atmospheric air](#)

Phys. Plasmas **19**, 033509 (2012); 10.1063/1.3692090

[Guiding of 35 TW laser pulses in ablative capillary discharge waveguides](#)

Phys. Plasmas **16**, 113105 (2009); 10.1063/1.3257909

[Measurement of ultrafast dynamics in the interaction of intense laser pulses with gases, clusters, and plasma waveguides](#)

Phys. Plasmas **12**, 056712 (2005); 10.1063/1.1885005

[Effective coupling of ultraintense laser pulse to funnel-mouthed plasma waveguides](#)

Phys. Plasmas **12**, 043105 (2005); 10.1063/1.1862248



Air plasma waveguide using pico-sec and nano-sec laser pulses

Pramod K. Pandey,¹ Shyam L. Gupta,¹ V. Narayanan,² and Raj K. Thareja^{1,a)}

¹*Department of Physics, Indian Institute of Technology Kanpur, Kanpur 208016 (U.P.), India*

²*Department of Physics, Indian Institute of Technology Rajasthan, Jodhpur, Rajasthan 342011, India*

(Received 25 August 2011; accepted 1 December 2011; published online 3 February 2012)

We report a shock driven plasma in air breakdown using pump-probe to elucidate the hydrodynamic evolution of air plasma waveguide. Imaging of the evolution of air plasma plume is used to investigate the pump pulse effect on the plume dynamic. Imaging of the channeled pulse through evolved waveguide shows five time enhancement in Rayleigh length at 7 ns delay of probe pulse with respect to pump pulse. The evolved channel radius $r_{ch} \approx 37 \mu\text{m}$ has been shown to couple the maximum energy of the probe pulse yielding the electron density difference $\Delta n_e \sim 10^{18} \text{ cm}^{-3}$ between axis and periphery of the channel. The air plasma wave guide is shown to support the fundamental mode at optimum delay. © 2012 American Institute of Physics.

[doi:10.1063/1.3676617]

I. INTRODUCTION

The abundant applications of plasma channeling such as laser wakefield accelerators,¹ high harmonic generation,² remote sensing,³ and advanced laser fusion schemes⁴ have attracted considerable interest in this field in the recent past. The pulsed-laser breakdown of air has been investigated extensively for many years because of its potential applications in remote sensing and communication.³ A high power laser beam focused in air causes the air breakdown due to cascade ionization/multiphoton ionization. The high temperature air plasma, thus formed, moves with the supersonic speed in the ambient air forming shock waves. The propagating shock wave moves away from the focal region and results in radially increasing electron density.⁵ A laser pulses can be guided through the plasma when the refractive index along the optical axis can be increased sufficiently to balance the diffraction effects due to focusing.⁵ However, the recombination between electrons and ions decreases radial electron density gradient which limits the channel life time,⁶ and hence make it unsuitable for the practical applications, which require channels not only long in terms of distance but also long life time. Thus for guiding of a pulse through the plasma, it is imperative that probe pulse be sent through the pre formed plasma with controlled delay with respect to plasma creating pulse such that it enhances the radial electron density gradient and suppresses the recombination processes in the plasma. This eventually results in increase of the life time of the plasma channel. The ten times enhancement in the life time of the plasma channel in air as compared to the single pulse case using femto-sec and subnano-sec laser pulses has been reported.⁷

Several techniques such as hollow capillaries, channeling by hydrodynamic expansion of a line focused discharge using axicon, z-pinch plasmas, gas filled capillary discharges, and relativistic guiding have been studied.^{8–10} The guiding of a high peak power pulse (fs) has been reported

using Kerr lensing where non linear intensity dependent refractive index of the medium acts as a positive lens that focuses the beam to overcome the diffraction effects due to ionization of the medium.⁷ However, the filamentation breaking of the beam at high intensity limits it to happen.¹¹

In the present work, we conclusively demonstrate the guiding properties of the preformed plasma waveguide for the second pulse, lengthening of the channel because of the redistribution of the radial electron density and movement of the shock radially outwards from the focal region. The paper is organized as follows: Section II describes the details of the experimental setup, the results and discussion are presented in Sec. III, and conclusions are given in Sec. IV.

II. EXPERIMENTAL

The schematic of the experimental setup used is shown in Fig. 1. In order to study the plasma channel formed in air, we used the Nd:YAG pico-second (ps) laser (Quantel:YG901C) of wavelength $\lambda = 1064 \text{ nm}$ and pulse width $\tau_p = 50 \text{ ps}$ (full width at half maximum, FWHM) and is referred as pump pulse P_1 . The laser consists of an active passive mode locked oscillator and double pass amplifier, which delivers maximum energy of 80 mJ at 10 Hz repetition rate. A nano-second Nd:YAG laser, pulse width of 6 ns (FWHM), having active Q-switched oscillator (Quanta Ray INDI) delivering maximum of 200 mJ at its second harmonic, $\lambda = 532 \text{ nm}$ with repetition rate of 10 Hz, was used as probe pulse P_2 . The pump pulse was focused to a spot size $r_0 = 10 \mu\text{m}$ to achieve a maximum intensity $\sim 2 \times 10^{14} \text{ W/cm}^2$ and stable air breakdown. A small part (<10%) of the pump beam P_1 was passed through a potassium dihydrogen phosphate (KDP) crystal to generate second harmonic (532 nm) beam P_3 for use in interferometry experiment. The residual $\lambda = 1064 \text{ nm}$ coming along with the $\lambda = 532 \text{ nm}$ after the KDP crystal was filtered out using a $\lambda = 532 \text{ nm}$ reflector [Item 6 shown in Fig. 1]. We have used Nomarski interferometer [NI, with components 11 to 13 as shown in Fig. 1]¹² to measure the electron density in the channel. The probe beam P_3 passing through Wollaston prism splits into two components with polarization perpendicular to

^{a)} Author to whom the correspondence should be addressed. Electronic mail: thareja@iitk.ac.in.

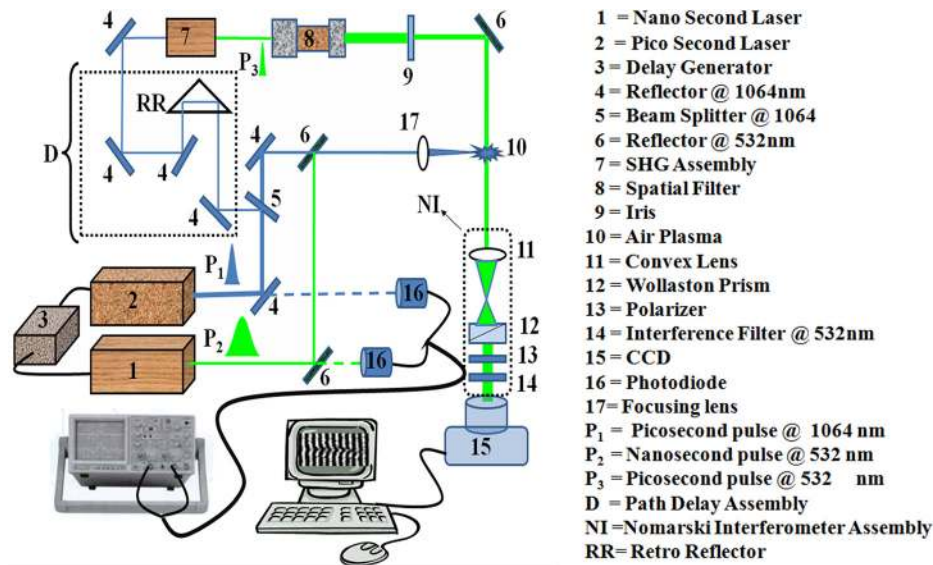


FIG. 1. (Color online) Experimental setup.

each other and then passes through the polarizer, whose transmission axis was oriented in such a way that both emergent beams have the same intensity, thus producing interference fringes with high contrast. The $\lambda = 532$ nm pass interference filter [refer Fig. 1 Item 14] was used to block the radiations other than probe beam coming from the plasma and to improve contrast of fringes. In order to record shadowgraphs, the polarizer [refer Fig. 1 Item 13] was rotated in such a way that it allows only one of the beams to pass. The delay between the pulse P_3 and pump pulse P_1 reaching at the focal spot [refer Fig. 1 Item 10] was created by giving the path difference using path delay assembly [D in Fig. 1]. The path difference between pulses P_1 and P_3 was monitored using photodiodes attached to the oscilloscope [not shown in the Fig. 1] kept at fixed position for a particular set of data. The pulse P_2 for heating the air plasma was sent collinearly with the pulse P_1 with a controllable delay using delay generator (SRS DG-535). The delay between the two pulses P_1 and P_2 was monitored using photodiodes [Item 16 refer Fig. 1] connected to the oscilloscope. Interferogram was imaged on to the charged coupled device (CCD) (LISAA-A1251 Apogee, USA) interfaced with the computer. The images, for which the delays between P_1 and P_2 , were exactly same as the prefixed time delay between P_1 and P_3 were recorded. The imaging of the channel was done by replacing Nomarski interferometer [Items 11–14 refer Fig. 1] and the CCD by triggered gated intensified charged coupled device (ICCD) (DH-720, ANDOR Technology, USA) interfaced with the computer. For the comparative study of the plume dynamics using nano-second and pico-second pulses, the air breakdown plume images created by using Nd:YAG nano-sec laser, wavelength $\lambda = 1064$ nm of pulse width 8 ns with intensity $\sim 8 \times 10^{12}$ W/cm² at the focal spot, were recorded using ICCD.

III. RESULTS AND DISCUSSION

As stated earlier, the guiding of laser pulse can be achieved using the hydrodynamic evolution of air breakdown at power levels much below the critical power (P_{crit}

$= \lambda^2/2\pi n_1 n_2 \sim 5.6$ GW for air, where λ is the laser wavelength, n_1 is refractive index of air, and $n_2 = 3.2 \times 10^{-19}$ cm²/W for air).⁷ We have earlier shown that the life time of the plasma channel can be increased by heating the pico-second laser produced air plasma using nano-second laser pulses.¹³ An intense laser pulse ($< P_{\text{crit}}$) focused in air causes the ionization in air either by cascade or by multiphoton ionization. We have used a typical pump-probe experiment, where pump beam creates air plasma that expands with local sound speed, creates a shock, and a probe beam heats it up making the beam self-channeled through the plasma.¹³ The pulse width (τ_p) of the laser used for creating the air spark plays a vital role to get the favourable environment for guiding. Fig. 2 shows images of the air plasma plume generated using 6 ns and 50 ps pulses of $\lambda = 1064$ nm at various times delays with respect to ablating pulse with focused intensity $\sim 8 \times 10^{12}$ W/cm² and $\sim 2 \times 10^{14}$ W/cm², respectively. It shows a distinct difference in the movement of the plume in the two cases. This peculiar expansion of plume is attributed to different ionization processes dominating for ns and ps pulses. It has been shown that cascade ionization is a dominant process for the evolution of the air plasma plume, whereas multiphoton-ionization dominates over cascade ionization in the case of ps laser breakdown of air.^{14–16} On focusing of ns pulses, the

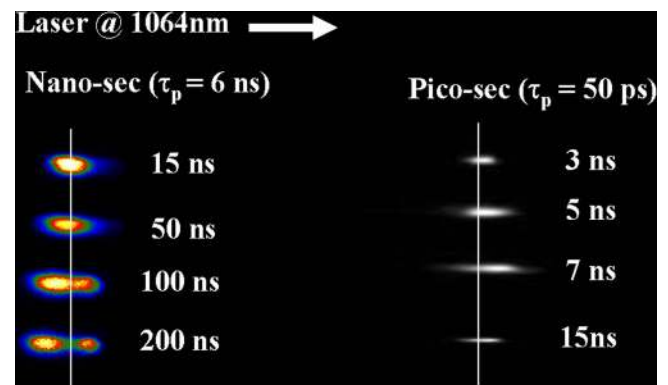


FIG. 2. (Color online) Air plasma evolution images using nano-sec and pico-sec lasers.

plume formed in the focal region sends a shock wave in all directions. The laser pulse energy is preferentially absorbed in that part of the shock wave which is moving towards the laser resulting in backward expansion of the plume as shown in Fig. 2. Whereas, in the case of ps-laser irradiation instantaneously released energy and momentum transfer of the radiation to the focal region drives a shock wave in the direction of the laser beam resulting in the plume expansion along the direction of the incident laser pulse. In order to further elaborate the effect of pulse width, we calculated the shock temperature T_{sh} and pressure P_{sh} for both cases. The evolved shock wave temperature and pressure can be estimated using¹⁷⁻¹⁹

$$T_{sh} = \frac{2\gamma}{\gamma + 1} \left[\frac{(\gamma - 1)}{(\gamma + 1)} \left(\frac{v_s}{c_0} \right)^2 + 1 \right] T_0, \quad (1)$$

$$P_{sh} = \frac{P}{\gamma + 1} \left[2\gamma \frac{v_s^2}{c_0^2} - \gamma + 1 \right], \quad (2)$$

where $\gamma \approx 1.2$ is the ratio of specific heats for air, v_s is shock front velocity, c_0 is the sound speed, and $T_0 = 300$ K is the background air temperature. The shock front velocity is calculated from the plume front position at various times of the expanding plume. For our case, the average plume front velocity is $v_s^{nano} = 1.0 \times 10^6$ cm/sec and $v_s^{pico} = 5.0 \times 10^6$ cm/sec with corresponding shock temperatures, $T_{sh}^{nano} = 2.3$ eV and $T_{sh}^{pico} = 58$ eV for ns- and ps-laser, respectively. Due to the lower shock temperature, the ns-laser ablated air plasma plume evolves slowly with channel evolution time ($\tau_c = \frac{r_0}{v_s}$, where r_0 is beam spot size and shock speed v_s in the medium) of 1.0 ns.⁵ This time is much shorter than the ablating pulse duration ($\tau_p = 6$ ns) and leads to an evenly distributed density profile and hence not favorable for plasma channel formation. The higher shock temperature $T_{sh}^{pico} = 58$ eV for ps plasma indicates that strong shock will evolve very quickly because of the very high shock pressure. The shock pressure of $p_{sh}^{pico} = 2.45 \times 10^4$ atm for our case is much higher than the ambient pressure and hence the air plasma continuously detonates and compresses the ambient air, the induced shock wave propagates at supersonic speed. Since the time scale for the channel evolution in this case (τ_c)_{ps} = 200 ps is much longer than the pulse duration ($\tau_p = 50$ ps), the plume moves forward and expands cylindrically away from the focal region due to the gained energy and momentum from the radiation.⁵ The cylindrical expansion of the shock wave results in radially increasing electron density, thereby forming a waveguide which can support a Gaussian beam injected after a controllable delay.^{5,9} Fig. 3 shows the plasma channel images taken using ICCD at different time delays between pump and probe pulses P_1 and P_2 . Fig. 4 shows the variation of the corresponding axial line intensities of the images. The delay between the two pulses is essential because the electron density takes some time to evolve for the efficient guiding of the injected pulse. The length of the plasma channel waveguide was maximum $L_w = 1.75$ mm when the pulse P_2 was sent at 7 ns of delay with respect to P_1 . The small delays between the pulses P_1 and P_2 results in short channel length, for the shock

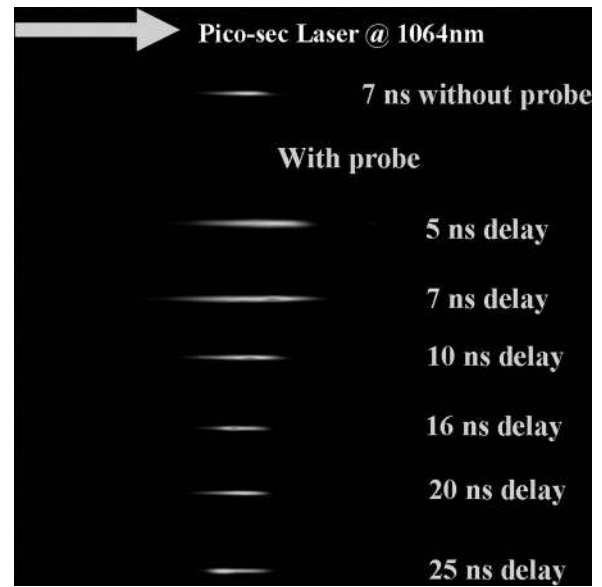


FIG. 3. Channel images with and without probe pulse.

wave remains within the focal region of the probe pulse. As the delay between the two pulses increases the shock wave moves radially out of the focal region and most of the pulse energy passes through the radially increasing central profile and hence enhanced inverse bremsstrahlung (IB) absorption and enhanced channel length. However, at longer delays, the injected pulse P_2 interacts with the decreasing electron density in the channel that results in reduced fractional enhancement in the electron density due to weak IB absorption and hence to short channel length. A slight hump in the axial intensity profile, Fig. 4 of the image at 7 ns delay may be due to the enhanced radially increasing central electron density profile that causes the beam of pulse P_2 to be lensed or converged as it leaves the channel. The resulting radially increasing electron density forms a plasma waveguide suitable for guiding has a parabolic electron density profile, $n_e(r) = n_e(0) + n_{cr} \left(\frac{r}{r_0} \right)^2$ for $r < r_{ch}$ and $n_e(r) = 0$ for $r > r_{ch}$, r_{ch} is channel radius.^{11,20} where r_0 is the laser spot size, $n_{cr} = \frac{m_e \omega^2}{4\pi e^2} \approx 10^{21}$ cm⁻³ for $\lambda = 1064$ nm is the critical

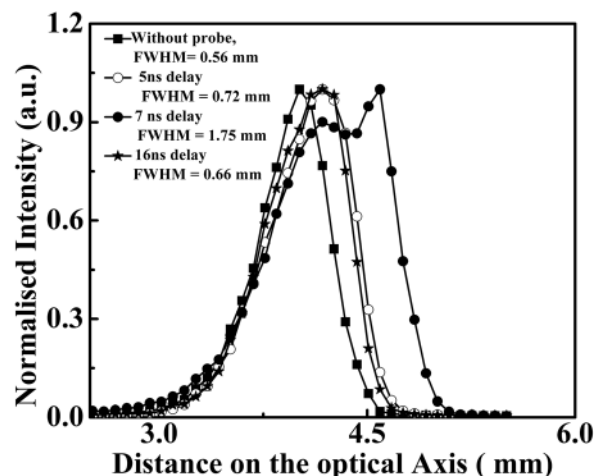


FIG. 4. Axial intensity profile of the channel images at different delays.

electron density, and $n_e(r)$ is the radial electron density. The corresponding refractive index is written as $n(r) \approx 1 - \frac{n_e(r)}{2n_{cr}}$. For a Gaussian laser beam to propagate through the parabolic plasma channel, the beam should be matched with the plasma channel radius. Following the evolution of channel radius equation,^{10,20} the condition for guiding of any mode with $r_s = r_0$, the corresponding refractive index difference is given by $\Delta n^{\min} = \frac{\lambda_{P_2}^2}{2\pi^2 r_0^2 n_0^2} \sim 1.4 \times 10^{-4}$ in our case, here $\lambda_{P_2} = 532 \text{ nm}$ and n_0 is the value of refractive index at the wave guide axis, $r = 0$. The corresponding electron density for guiding the Gaussian pulse of spot size r_0 through the plasma channel becomes $\Delta n_e = \frac{1}{\pi r_e r_0^2}$, where r_e is the classical electron radius.^{5,13} For our experimental conditions ($r_0 = 10 \mu\text{m}$), we get $\Delta n_e = 1.13 \times 10^{18} \text{ cm}^{-3}$.

In order to measure the spatial variation of electron density of the plasma channel evolution at different time delays a Nomarski interferometer¹² as shown in Fig. 1 has been designed. The second harmonic $\lambda = 532 \text{ nm}$ of the Nd: YAG pico-sec laser pulse P_3 was used for interferometry probe. The interferogram and corresponding shadowgram were recorded through the CCD camera. The interferogram of air plasma channel evolution at different time delays after pump pulse P_1 (without probe pulse P_2) were recorded. Fig. 5 shows interferograms and their corresponding shadowgrams at delay of 2.5, 3.0, and 7.0 ns, respectively, after the pump pulse P_1 .

The analysis of electron density profile is done using Abel inversion.^{21–23} Fig. 6 shows the calculated radial electron density profile at various time delays with and without probe pulse P_2 . The electron density initially increases radially because of expansion of shock front in air plasma with the energy stored in it resulting in further ionization. However, at later times, the density decreases due to loss in energy by the collisions among electrons, atomic, and ionic species. The recombination of electrons with the oxygen molecules to form O^- and O_2^- in air also contributes to decrease in electron density at later times.¹³ The pulse P_2 having energy just below the threshold for air breakdown sent through the plasma heats the plume resulting in suppression of the recombination with the oxygen molecules

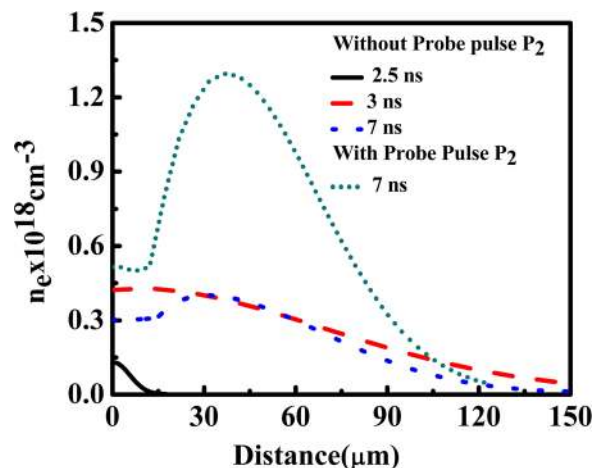


FIG. 6. (Color online) Evolution of electron density, with and without probe pulse at different delays.

and hence increase in the radial electron density. In order to investigate the channel formation, the time delay between the pump pulse P_1 and the probe ns-pulse P_2 was varied in steps. Following Fig. 6, it is clear that radial electron density and hence channel radius r_{ch} evolves as the delay increases. At initial delays, r_{ch} is not broad enough to couple the probe pulse P_2 and most of the pulse energy is lost outside the channel. However, at longer delays (greater than 7 ns), the injected pulse P_2 may interact with the decreasing electron density in the channel that results in weak IB absorption and reduced enhancement in the electron density. Fig. 7 shows the radial as well as longitudinal (lateral) variation of electron density and corresponding refractive index profiles for the plasma channel evolved at 7 ns delay with and without probe pulse P_2 . It is observed from the images of the plasma channel and shadowgram, Fig. 5, that delay of 7 ns shows five times enhancement in the Rayleigh length $z_0 = \frac{\pi r_0^2}{\lambda} = 0.3 \text{ mm}$.

Since, the experimentally created plasma channel do not have infinitely high walls (i.e., densities), the channel walls reach a peak height at a finite radius beyond which the density rapidly falls to zero. The laser modes are quasi-bound or leaky in such a channel and can tunnel through the channel

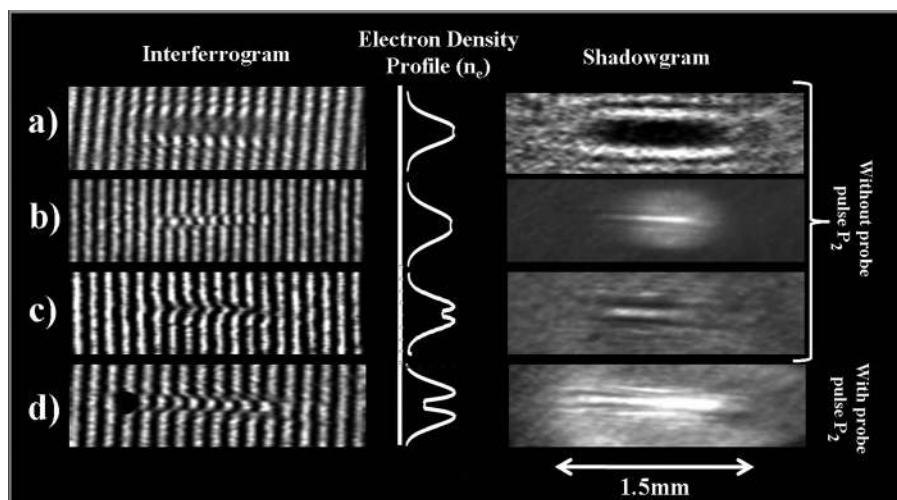


FIG. 5. Interferogram and corresponding electron density profile and shadowgrams of air plasma at different delays (without probe pulse P_2) (a) 2.5 ns (b) 3 ns (c) 7 ns, and (d) with probe pulse P_2 at 7 ns delay.

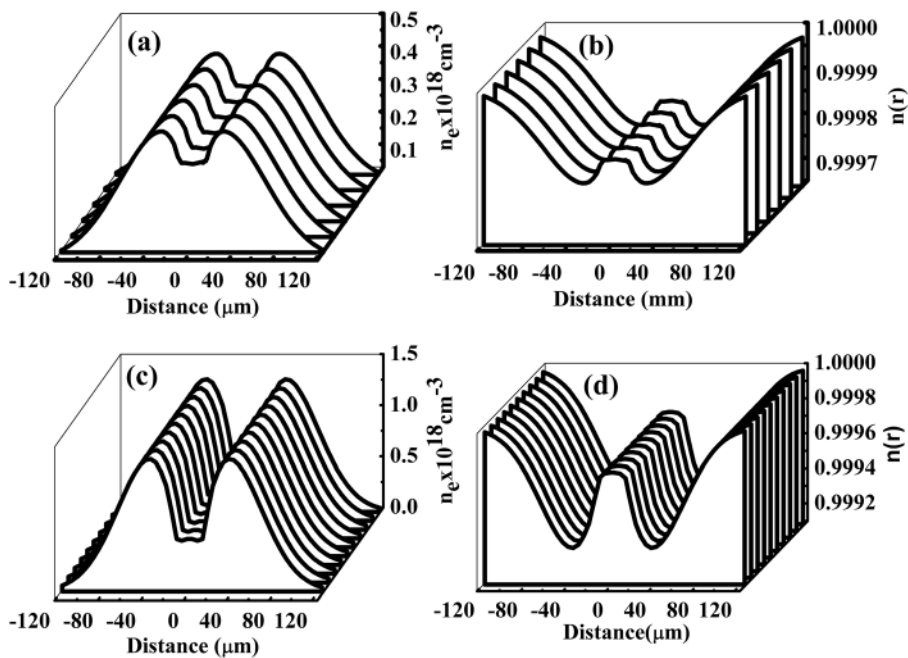


FIG. 7. Electron density and refractive index profiles at 7 ns delay without probe pulse (a, b) and with probe pulse (c, d).

walls and couple to the continuum.²⁰ The leakage rate depends upon the channel parameters and the channel mode profile.²⁰ It has been shown²⁰ that for a parabolic channel of radius r_{ch} , the laser modes can tunnel through if $r_{ch}^2 > \{(2m + p + 1) + [(2m + p + 1)^2 - p^2]^{1/2}\} \frac{r_0^2}{2}$, where p and m are radial and azimuthal mode indices. Thus for the fundamental mode ($m = p = 0$) to propagate, the channel radius should be greater than the laser spot size r_0 . In our case, the measured channel radius ($r_{ch} \sim 37 \mu\text{m}$) is greater than the laser spot size; thus, the channel formed at 7 ns delay is suitable for the fundamental mode guiding. In order to further confirm the guiding of the mode through the plasma channel, we calculated the parameter V , $V = \frac{\omega_p r_{ch}}{c}$ which defines how many modes a waveguide can support.²⁴ It follows that the optimum density of the plasma channel which supports a single mode calculated for our experimental conditions is $n_e \approx 0.12 \times 10^{18} \text{ cm}^{-3}$, in agreement with measured electron density at 7 ns delay [Fig. 7(a)]. Fig. 8 shows the mode profile at the waveguide exit at 7 ns delay.

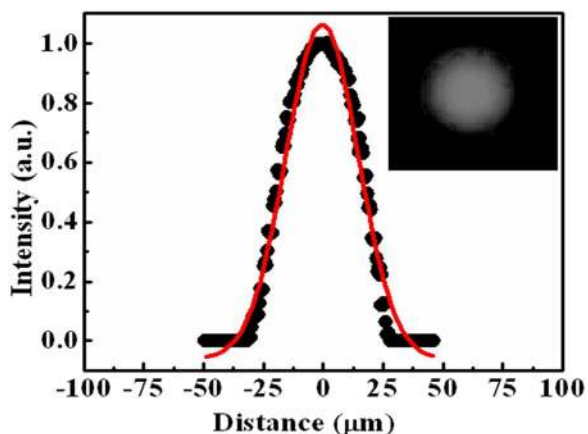


FIG. 8. (Color online) Mode profile at the channel exit.

IV. CONCLUSION

We studied the role of the pulse width of the laser in the formation of the plasma channel. It is observed that a plasma channel could be formed using hydrodynamic expansion of ps laser created plasma. It has been shown that electron density takes some time to evolve as a plasma waveguide in which another pulse can be guided. The guiding pulse suppresses the recombination processes and tailors the electron density of the plasma waveguide for the self guiding. The prolongation in Rayleigh length of the plasma channel up to a factor of five was observed when the ns-pulse was sent at delay of 7 ns with respect to ps-pulse. The waveguide is shown to sustain single mode propagation at an optimum delay of propagating pulse.

- ¹C. G. R. Geddes, Cs. Toth, J. van Tilborg, E. Esarey, C. B. Schroeder, D. Bruhwiler, C. Nieter, J. Cary, and W. P. Leemans, *Nature* **431**, 538 (2004).
- ²X. F. Li, A. L' Huillier, M. Ferray, L. A. Lompre, and G. Mainfray, *Phys. Rev. A* **39**, 5751 (1989).
- ³J. Kasparian, M. Rodriguez, G. Méjean, J. Yu, E. Salmon, H. Wille, R. Bourayou, S. Frey, Y. B. André, A. Mysyrowicz, R. Sauerbrey, J. P. Wolf, and L. Wöste, *Science* **301**, 61 (2003).
- ⁴A. Pukhov and J. Meyerter-Vehn, *Phys. Plasmas* **5**, 1880 (1998).
- ⁵C. G. Durfee III, J. Lynch, and H. M. Milchberg, *Phys. Rev. E* **51**, 2368 (1995); *Opt. Lett.* **19**, 1937 (1994).
- ⁶S. Tzortzakos, B. Prade, M. Franco, and A. Mysyrowicz, *Opt. Commun.* **181**, 123 (2000).
- ⁷Z. Q. Hao, J. Zhang, Y. T. Li, X. Lu, X. H. Yuan, Z. Y. Zheng, Z. H. Wang, W. J. Ling, and Z. Y. Wei, *Appl. Phys. B* **80**, 627 (2005).
- ⁸F. Dorchies, J. R. Marqués, B. Cros, G. Matthieussent, C. Courtois, T. Vélikorousov, P. Audebert, J. P. Geindre, S. Reibibo, G. Hamoniaux, and F. Amiranoff, *Phys. Rev. Lett.* **82**, 4655 (1999).
- ⁹C. G. Durfee III and H. M. Milchberg, *Phys. Rev. Lett.* **71**, 2409 (1993).
- ¹⁰E. Esarey, P. Sprangle, J. Krall, and A. Ting, *IEEE J. Quantum Electron* **33**, 1879 (1997).
- ¹¹A. Couairon and A. Mysyrowicz, *Phys. Rep.* **441**, 47 (2007).
- ¹²J. Ruiz-Camacho, F. N. Beg, and P. Lee, *J. Phys. D: Appl. Phys.* **40**, 2026 (2007).
- ¹³V. Narayanan, V. Singh, P. K. Pandey, N. Shukla, and R. K. Thareja, *J. Appl. Phys.* **101**, 073301 (2007).

- ¹⁴Yu. P. Raizer, *Soviet Phys. Uspekhi* **8**, 650 (1966).
¹⁵C. G. Morgan, *Rep. Prog. Phys.* **38**, 621 (1975).
¹⁶R. Tambay and R. K. Thareja, *J. Appl. Phys.* **70**, 2890 (1991).
¹⁷A. K. Sharma and R. K. Thareja, *Appl. Phys. Lett.* **84**, 4490 (2004).
¹⁸P. E. Dyer, A. Issa, and P. H. Key, *Appl. Phys. Lett.* **57**, 186 (1990).
¹⁹Yan Qian, Jian Lu, and Xiaowu Ni, *Chin. Opt. Lett.* **7**, 410 (2009).
²⁰T. R. Clark and H. M. Milchberg, *Phys. Rev. Lett.* **78**, 2373 (1997); *Phys. Rev. Lett.* **81**, 357 (1998); *Phys. Rev. E* **61**, 1954 (2000).
²¹S. L. Jackson and U. Shumlak, *Rev. Sci. Instrum.* **77**, 083502 (2006).
²²R. Illingworth and R. K. Thareja, *J. Phys. E: Sci. Instrum.* **14**, 147 (1981).
²³K. Bockasten, *J. Opt. Soc. Am.* **51**, 943 (1961).
²⁴H.-M. Shen, *J Appl. Phys.* **69**, 6827 (1991).